HHS Public Access

Author manuscript

Cell Host Microbe. Author manuscript; available in PMC 2017 November 29.

Published in final edited form as:

Cell Host Microbe. 2015 February 11; 17(2): 178–190. doi:10.1016/j.chom.2014.12.008.

Stressed mycobacteria use the chaperone ClpB to sequester irreversibly oxidized proteins asymmetrically within and between cells

Julien Vaubourgeix[1], **Gang Lin**[1], **Neeraj Dhar**[2], **Nicolas Chenouard**[4], **Xiuju Jiang**[1], **Helene Botella**[1], **Tania Lupoli**[1], **Olivia Mariani**[3], **Guangli Yang**[5], **Ouathek Ouerfelli**[5], **Michael Unser**[3], **Dirk Schnappinger**[1], **John McKinney**[2], and **Carl Nathan**[1,*]

[1]Department of Microbiology and Immunology, Weill Cornell Medical College, 1300 York Avenue, New York, New York 10065, USA [2]School of Life Sciences, Swiss Federal Institute of Technology in Lausanne (EPFL), SV 3834, Station 19, CH-1015 Lausanne, Switzerland [3]Biomedical Imaging Group, Swiss Federal Institute of Technology in Lausanne (EPFL), BM 4.134, Station 17, CH-1015 Lausanne, Switzerland [4]Department of Physiology and Neuroscience, New York University, Langone Medical Center, 450 East 29th Street, New York, NY 10016, USA [5]Organic Synthesis Core Facility, Molecular Pharmacology and Chemistry Program, Memorial Sloan-Kettering Cancer Center, 430 East 67th Street, New York, NY 10065, USA

SUMMARY

Mycobacterium tuberculosis (Mtb) defends itself against host immunity and chemotherapy at several levels, including the repair or degradation of irreversibly oxidized proteins (IOPs). To investigate how Mtb deals with IOPs that can neither be repaired nor degraded, we used new chemical and biochemical probes and improved image analysis algorithms for time-lapse microscopy to reveal a defense against stationary phase stress, oxidants and antibiotics— the sequestration of IOPs into aggregates in association with the chaperone ClpB, followed by the asymmetric distribution of aggregates within bacteria and between their progeny. Progeny born with minimal IOPs grew faster and better survived a subsequent antibiotic stress than their IOP-burdened sibs. ClpB-deficient Mtb had a marked recovery defect from stationary phase or antibiotic exposure and survived poorly in mice. Treatment of tuberculosis might be assisted by drugs that cripple the pathway by which Mtb buffers, sequesters and asymmetrically distributes IOPs.

INTRODUCTION

Mycobacterium tuberculosis (Mtb) can persist in the human host in a latent state for decades, reflecting the partial success of a host immune response that keeps about 90% of infected but immunocompetent people from developing clinically active tuberculosis (TB). When TB does develop but goes untreated, the pathogen takes about 3 years to kill about

*Address correspondence to: Carl Nathan, Department of Microbiology and Immunology, Weill Cornell Medical College, 1300 York Avenue, New York, New York 10065, USA. Phone: 212.746.6505; Fax: 212.746.8587; cnathan@med.cornell.edu.

70% of its hosts (Tiemersma et al., 2011). When active TB is drug-sensitive, combination chemotherapy takes about 6 months to cure 95% of cases, while optimal treatment regimens for drug-resistant TB average 27 months (Ahuja et al., 2012). These dismal statistics suggest that Mtb, the single leading cause of death from bacterial infection, can survive for prolonged periods under stresses imposed by the host, by antibiotics, or both. Understanding how Mtb handles such stresses may suggest new ways to impair its ability to do so.

The mechanisms have only begun to emerge that Mtb uses to withstand host-imposed stresses, such as exposure to reactive oxygen species (ROS), reactive nitrogen species (RNS), carbon monoxide, acid, cupric ions and antimicrobial peptides, as well as deprivation of oxygen, iron and nutrients, all of which impact multiple pathways. Mtb's defenses against host-imposed stresses include catabolizing ROS and RNS (Bryk et al., 2002), repairing their damage (Mazloum et al., 2011), and degrading damaged macromolecules that cannot be repaired (Lin et al., 2009).

We predicted that Mtb is likely to deploy yet another form of defense to protect itself from the toxicity of damaged macromolecules that can neither be repaired nor degraded. We focused on heavily oxidized proteins that irreversibly accumulate carbonyls on amino acid side chains (Figure 1A) (Dukan and Nyström, 1998). Irreversibly oxidized proteins (IOP) tend to mis-fold, exposing hydrophobic regions that foster aggregation; to cross-link; and to gain toxic functions through illicit binding (Hartl et al., 2011). If oxidation is extensive enough, IOP can escape degradation by resisting the unspooling process that feeds polypeptide chains into chambered proteases (Grune et al., 2004). Moreover, they can titrate chaperones away from essential tasks, such as assisting in the folding of nascent polypeptides. Thus, it seems that cells that are adept at withstanding severe, prolonged stress must find a way to minimize the adverse impact of IOP.

Here, application of chemical, biological and computational tools revealed that mycobacteria protect themselves from diverse stresses by asymmetrically distributing IOP intracellularly, and then asymmetrically distributing the collected IOP between progeny when the parental cells divide. Progeny that inherit more IOP grow more slowly than those that inherit less and are more likely to die when exposed to antibiotics again. ClpB emerged as both a marker of IOP and a mediator of resistance against proteotoxic stress. Mtb that lack ClpB are less fit to recover from stationary phase or antibiotic exposure *in vitro* and are less virulent in mice than their wild-type and complemented counterparts.

RESULTS

Identification of IOP in stressed mycobacteria and association with ClpB

Protein-associated carbonyls are often detected through formation of hydrazones on exposure to 2,4-dinitrophenylhydrazine, as monitored by spectrophotometry or anti-DNP immunoblot (Figure S1A and S1B). We used these methods to demonstrate that protein-associated carbonyls markedly increased in stationary phase compared to log phase cells of *Mycobacterium smegmatis* (Msm) (Figure S1C), *Mycobacterium bovis* var. Calmette-Guérin (BCG) (Figure S1D) and Mtb (Figure 1B). Carbonyls also accumulated upon exposure of Mtb to H_2O_2 alone or in combination with acidified nitrite—a source of RNS—

or starvation (Figure 1B). Quantitative comparisons were not feasible, because the products were largely insoluble, even in SDS, guanidine-HCl or urea.

To identify proteins undergoing carbonylation, we subjected Mtb to starvation, prolonged stationary phase, H_2O_2, acidified $NaNO_2$, or H_2O_2 in acidified $NaNO_2$. We used beads bearing a hydrazide to covalently capture carbonylated proteins and identified 67 of them from their tryptic peptides (Figure S1E). Five of the high-scoring candidates were homologs of IOP in other bacteria (Figure S1E) (Dukan et al., 2000; Dukan and Nyström, 1999; Tamarit et al., 1998). The top-ranked IOP was the nucleoid-associated protein HupB (Rv2986c), an iron-storage protein with ferroxidase activities that protects DNA from oxidative damage (Takatsuka et al., 2011), perhaps at its own expense.

To render IOP detectable in intact mycobacteria and visualize their distribution, we synthesized cell-penetrant probes that link fluorescein isothiocynate (FITC) or Texas Red (TR) to 15-amino-4,7,10,13-tetraoxapentadecanoic acid hydrazide (ATPAH), which will react with carbonyls (Figure 1C and 1D). Next, we used HupB to explore the fate of a protein in mycobacteria when some of its copies undergo irreversible oxidation. We transformed Mtb with a functional HupB-fluorescent protein fusion construct (ID#3 in Table S1, Figure S1F and S1G) and compared HupB's distribution in log and stationary phases. In log phase Mtb, HupB and the nucleoid both extended along much of the cell's longitudinal axis. In late stationary phase, 47.2% of 106 HupB foci scored colocalized with the shortened nucleoid, but 38.7% of HupB foci that reacted with the probe for carbonyls relocated at a distance from it (Figure 1E). Thus late stationary phase caused some portion of HupB to become carbonylated, to aggregate and to redistribute.

This approach did not allow us to generalize from the behavior of one protein to the behavior of IOP in general. As a method to monitor the distribution of IOP as a class, we tagged and tracked a chaperone and demonstrated its interaction with IOP using a chemical probe.

Association of ClpB with IOP

In yeast, parental cells retain carbonylated proteins and accumulate them with replicative age (Aguilaniu et al., 2003). Asymmetric distribution of IOP involves the disaggregase Hsp104 (Coelho et al., 2014; Erjavec et al., 2007; Hill et al., 2014; Liu et al., 2010), which is not itself an IOP. ClpB, Hsp104's homolog in *E. coli*, unwinds mis-folded proteins prior to re-folding by DnaK/J co-chaperones (Glover and Lindquist, 1998; Goloubinoff et al., 1999; Motohashi et al., 1999; Rosenzweig et al., 2013). We thus evaluated whether we could use the distribution of ClpB as a proxy for the distribution of IOP as a class. We replaced endogenous ClpB in Msm and Mtb with functional Mtb's *clpB-gfp* (Figure S2 and S3A, and Table S1, ID#7 & 11), and applied the probe for carbonylated proteins to cells from log and stationary phase cultures. TR-ATPAH only stained log-phase Msm and Mtb diffusely at the cell surface. In contrast, the probe brightly stained 71.1% of 121 ClpB-GFP aggregates within Mtb in stationary phase; results were similar with Msm (Figure 2A and S3B).

To track the emergence and distribution of IOP within a cell and from parental cells to descendants, we turned to time-lapse microscopy (TLM). This imposed the need for a

stressor that could be rapidly introduced and removed, unlike stationary phase, and would not degrade a fluorescent signal, like H_2O_2 (Winter et al., 2005).

We treated Msm:Δ*clpB*sm::*clpB-gfp* cells (Table S1, ID#7) with a proteotoxic stressor—kanamycin at sub-growth-preventing concentrations of 0.25 or 1 μg/mL—based on evidence that when translation fidelity is corrupted, aberrant proteins accumulate that are prone to carbonylation (Dukan et al., 2000; Ling et al., 2012). We lysed the mycobacteria and found reactivity with FITC-ATPAH chiefly in the sedimentable fraction, indicating that IOP were aggregated (Figure 2B). Likewise, ClpB-GFP accumulated chiefly in the sedimentable fraction (Figure 2C). This suggested either that ClpB was itself aggregated, or that it associated with aggregates of other proteins. Treatment of Msm:Δ*clpB*sm::*clpB-gfp* with either or both kanamycin (1 μg/mL) and disuccinimidyl glutarate (DSG), a cross-linking agent, revealed that ClpB-GFP associates noncovalently with aggregated IOP (Figure 2D).

To confirm the impression that diffusely distributed molecules of ClpB joined aggregates, we codon-adapted *dendra2* so that the protein expressed in mycobacteria switched emission from green to red after exposure to 405-nm light (Figure S3C to S3H) (Gurskaya et al., 2006). The initial distribution of ClpB appeared homogeneous (Figure 2E). In contrast, after kanamycin treatment of Msm:Δ *clpB*sm::*clpB-gfp* or Msm:Δ *clpB*sm::*clpB-dendra2* (Table S1, ID#8), ClpB was distributed in aggregates (Figure 2E). When we lasered cells at the pole opposite their largest aggregate (as in Figure 2F, left), the aggregates converted their fluorescence from green to red at rates inversely proportional to their distance from the targeted region (Figure 2F, right & 2G). Thus ClpB from the cytoplasmic pool diffused to join the aggregates.

We concluded that we could use fluorescently tagged ClpB to track IOP in living mycobacteria.

Association of ClpB with aggregates in response to sublethal kanamycin at the microcolony level

Clinical dosing with antibiotics confronts Mtb with intermittent exposure to high concentrations, followed by exposure to sublethal concentrations. Some drugs may only achieve sublethal concentrations in cavities (Dartois, 2014). The ability of bacteria to adapt to intermittency of stress can determine the population's tolerance (Fridman et al., 2014). With this in mind, we applied a rest-stress-rest-stress-rest paradigm to the Msm strains Δ*clpB*Sm::*clpB-gfp* and Δ*clpB*Sm::*clpB-dendra2*, where "rest" means perfusion with drug-free medium, without implication as to metabolic state (Figure 3A; Movie S1).

During phase I, ClpB-Dendra's fluorescent signal was homogeneously distributed within the cytoplasm (Figure 3B, first panel: 2.5 h), as reflected by the mean number of aggregates per bacterial pixel being 3.3×10^{-5} (Figure 4A).

Application of sublethal kanamycin for 2 h (Phase II) led to an abrupt increase in the number of visible ClpB aggregates, peaking at 8.4×10^{-3} aggregates per bacterial pixel 60 minutes after the onset of the next drug-free period (Phase III) and then decreasing (Figure 3B, 4A and S4A) (de Chaumont et al., 2012; Olivo-Marin, 2002). As fluorescence intensity

increased at focal locations, it decreased elsewhere in the cells by an equivalent amount (Figure 4B), adding evidence that aggregates formed through redistribution of ClpB. About 16 h after removal of kanamycin, the number of aggregates per microcolony began to increase slightly as the microcolony resumed growing (Figure 3B and 4A). Far fewer additional aggregates formed on the second challenge with kanamycin, as reflected by constancy in the mean number of aggregates per bacterial pixel from the onset of the challenge to 60 minutes after its end ($\mu = 4.3\times10^{-3}$; $\sigma = 2.9\times10^{-4}$), perhaps reflecting kanamycin's interference with synthesis of new ClpB-GFP (Figure 4A and 4C).

We next characterized aggregates by size and binned the number of bacterial pixels occupied by each aggregate in 6 size classes. After the first exposure to kanamycin, the number of small aggregates fell as the number of large aggregates rose (Figure 4D). Quantification confirmed coalescence of small aggregates into bigger ones (Figure 4B). Large aggregates further re-localized within a cell. During and immediately after removal of kanamycin, aggregates appeared to be randomly distributed along the cell's length. However, by the end of the first post-kanamycin drug-free period, 60% of the aggregates lay within 10% of a cell's length from one of its poles (Figure 4E).

We monitored the growth of bacterial microcolonies by the increase in pixels that they occupied (Figure S4B and S4C). By design, the first exposure to kanamycin slowed growth but did not halt it (Figure 4F). In contrast, the second exposure to kanamycin at the same concentration led to a heterogeneous response. Some cells stopped growing, turned phase dark and often proceeded to lyse, while others grew slowly. The median response approximated stasis (Figure 4F).

The post-peak decline in aggregates per bacterial pixel (Figure 4A) reflected aggregate fusion (Figure 4B and 4D) but likely also some combination of the following: reduced synthesis of ClpB-GFP; refolding or degradation of proteins that had entered aggregates; departure of ClpB-GFP from aggregates without replacement; or denaturation of some of the GFP or Dendra tags. For simplicity, we will refer to diminution in the intensity of aggregate-associated signal as "resolution".

To test whether ClpB's association with aggregates depends on its ability to bind substrate proteins, we considered that yeast Hsp104 requires each of two tyrosine residues in order to bind substrates, although not to hexamerize (Weibezahn et al., 2004). We transformed Msm with *clpB-gfp* ^{251}Tyr-to-^{251}Ala mutant (Y251A-GFP, ID#13, Table S1). To avoid toxicity from constitutive expression of mutant ClpB, we induced expression of the mutants by addition of anhydrotetracycline (Atc) 14h before exposure to kanamycin. The Y251-GFP mutant was induced (Figure S4D), but did not join aggregates in response to kanamycin (Figure 4G; Movie S2). In contrast, wild-type ClpB-GFP induced to similar levels joined aggregates (Figure 4H, Table S1, ID#12; Movie S3).

To establish that not any multimeric protein would join kanamycin-induced aggregates, we transformed Msm with the proteasome subunits *prcB* and *prcA*, adding mCherry to PrcA's C-terminus (Table S1, ID#17). PrcA-mCherry was induced (Figure S4E) by Atc but did not form visible aggregates in response to kanamycin (Figure 4I; Movie S4). Nor did GFP itself

join kanamycin-induced aggregates (Figure 4J, Table S1, ID#14; Movie S5). Thus, the ability to join IOP-containing aggregates was a relatively selective property of ClpB that depended on tyrosine 251.

In sum, quantitation revealed that aggregates rapidly formed following exposure to kanamycin and then decreased in number in large part through fusion but potentially also through resolution. In fact, inspection gave the impression that aggregates formed, fused, resolved and formed again in individual cells over time, which is not reflected in statistics for microcolonies. Thus, we carried the analysis to the single cell level.

Behavior of aggregates within individual cells and their asymmetric distribution to progeny

We assigned each aggregate a score, S_a, equal to the product of its mean intensity and size, summed scores for individual aggregates, and plotted cell length and the sum of S_a as functions of time. Cells whose S_a remained <2000 AU grew at the same rate as unstressed cells (data not shown), indicating that there was a threshold for the impact of S_a on growth.

Distribution of aggregates to descendants was asymmetric about 43% of the time at a kanamycin concentration of 1 μg/mL (Figure 5A). Figures 5 B, C, D and E illustrate the 4 major stereotypic patterns that were observed in roughly 42%, 8%, 17% and 33% of individual cells studied, respectively, at a kanamycin concentration of 1 μg/mL. The proportion of cells in pattern 1 rose when the concentration of kanamycin was increased to bactericidal levels (2 μg/mL). The proportion in pattern 4 rose when the concentration of kanamycin was reduced to 0.1 μg/mL.

In pattern 1, a cell that had been growing during the kanamycin exposure stopped growing afterwards, resolved and reformed aggregates and eventually achieved a fluorescence-free state, but this was associated with loss of all fluorescence and assumption of a phase-dark appearance that probably connoted death. Such cells neither resumed growth nor divided (Figure 5B).

In pattern 2, a cell that had not resolved its aggregates prior to cytokinesis distributed all or most of them (Figure 5C) to one descendant, which then lysed. The other, containing no aggregates, elongated at a nearly normal rate.

In pattern 3, one descendant had a far higher S_a score than the other, although the number of aggregates in each was the same (Figure 5D); the more burdened cell grew much more slowly than its sibling.

In the fourth pattern, descendants inherited nearly equal aggregate burdens and grew at nearly equal rates (Figure 5E).

In cells with any of these phenotypes, the number of aggregates and S_a fluctuated. This suggested that cells cycled through rounds of collection and sequestration of IOP and could resolve some aggregates.

The progeny of kanamycin-stressed parents that had higher IOP scores than their sibs tended to have slower elongation velocities (Kendall's correlation coefficient $\tau = -0.46$, $p = 8.24\times10^{-10}$) and tended to be longer at birth ($\tau = 0.31$, $p = 3.56\times10^{-5}$) (Figure 5F), contrasting with unstressed mycobacteria, for which elongation velocity positively correlated with length at birth (Santi et al., 2013; Wakamoto et al., 2013).

Next, we asked if divergent outcomes from the first kanamycin exposure were associated with different cell fates upon a second exposure. Indeed, cells with faster elongation velocities at T>15 hours in the first post-kanamycin rest period were more likely to divide at least once in the rest period following a second kanamycin exposure than cells with slower elongation velocities (Figure 5G).

Collectively, these results suggested that coalescence of small aggregates into progressively larger ones first generated and then exaggerated asymmetric distribution within a cell. Asymmetric distribution of aggregates in a parental cell favored asymmetric distribution of aggregates between its progeny. Inheritance of aggregates imposed a fitness cost with respect to subsequent cell elongation rate. Cells that elongated at higher velocities toward the end of the rest period following the first exposure to kanamycin better withstood a second exposure to the same stress.

Asymmetric distribution of ClpB in response to INH

We next explored if asymmetric distribution of ClpB-associated collections extended to an antibiotic with a different mechanism of action. We challenged Msm:Δ *clpBSm*::*clpB-gfp* or Msm:Δ *clpBSm*::*clpB-dendra2* in microfluidic chambers with isoniazid (INH) using a rest-stress-rest-stress perfusion paradigm (Figure 6A and Movie S6). INH markedly reduced microcolony growth (Figure 6B and C) and augmented the mean intensity of ClpB fluorescence, which peaked 30 minutes after removal of the drug (Figure 6D). ClpB formed patches after exposure to INH, in contrast to the discrete aggregates seen in response to kanamycin. During the Phase III drug-free period, the microcolony's size increased faster than the ClpB-GFP signal (Figure 6C), resulting in a drop of the mean fluorescent signal 30 minutes after the onset of phase III (Figure 6D). This was associated with a gain of heterogeneity of the mean intensity of fluorescence at the microcolony level, reflected in the increase in its coefficient of variation, C_v (Figure 6D).

During phase III, parental cells frequently gave rise to one progeny containing abundant patches of ClpB and another with little or no visible ClpB (Figure 6B). Patched ClpB sometimes concentrated in one half of a parental cell before cytokinesis was apparent (Figure 6B, T = 5 h, yellow arrows). Using the BisQuit ImageJ plugin for semi-automatic single-cell segmentation, we plotted the absolute value of the difference of ClpB's intensities in 178 INH-treated progeny pairs as a function of time (Figure 6E). This value was significantly different from 0 ($p < 0.004$), denoting asymmetric distribution.

Thus, sublethal exposure to a front-line TB drug with a mechanism of action distinct from that of aminoglycosides induced asymmetrical distribution of patches of ClpB within mycobacteria and between their progeny. Inheritance of aggregated ClpB was more consistently and extensively asymmetric following exposure to INH than following exposure

to kanamycin. This was so, even though aggregation of ClpB in response to INH did not proceed to such an extent that asymmetric distribution of aggregates became inescapable through their coalescence to small, odd numbers, as often seen with kanamycin.

Contribution of ClpB to mycobacterial fitness

To test the functional impact of ClpB in stressed mycobacteria, we assessed the fate of ClpB-deficient cells emerging from IOP-generating stresses in vitro or when confronted by conditions in a mammalian host. Deletion of *clpB* in Msm and Mtb (Figure S2, Table S1, ID#4 and #10) established that *clpB* was not essential for growth. The Mtb deletion mutant grew more slowly than wild type on 7H11 agar plates and formed smaller colonies, but grew at the same rate as wild type Mtb and the complemented strain (H37Rv:Δ*clpB::ClpB*) in liquid culture when diluted from logarithmic or early stationary phases (Figure 7A). In contrast, after reaching late stationary phase, Δ*clpB* Mtb cells had a marked recovery defect associated with a marked accumulation of carbonylated material (Figure 7B). Likewise, although wild type H37Rv Mtb, H37Rv:Δ *clpB*, and H37Rv:Δ *clpB::ClpB* were equally sensitive to growth inhibition by kanamycin and streptomycin (Figure S5A), Δ*clpB* Mtb recovered much more slowly than the control strains from exposure to sub-inhibitory concentrations of aminoglycosides (Figure S5B).

In mice, the ClpB-deficient mutant strain did not attain the same level of viable bacteria in the lungs as the wild type or the complemented strains, and did not persist at the maximal level attained, resulting in a 2 $\log_{10}$ lower burden of CFU at 4 months post-infection (Figure 7C) and markedly less pulmonary pathology than for wild-type Mtb or the complemented mutant (Figure 7D).

DISCUSSION

To the multiple layers of Mtb's defenses, the present observations add what may be a defense of last resort: sequestration of proteins whose irreversible accumulation of carbonyls leads to mis-folding. Mis-folding may make proteins as dangerous as they are resistant to degradation by the two major chambered proteases of Mtb, ClpP1P2 (Raju et al., 2012) and the proteasome (Darwin et al., 2003; Lin et al., 2009). IOP that are resistant to degradation can accumulate as potentially proteotoxic species.

Bacterial cells that reproduce by binary fission could dispose of non-degradable IOP in at least three ways, as outlined in Figure S6. Among these, aggregation of IOP and their asymmetric distribution between progeny is emerging as a widespread means by which a parental cell can rejuvenate one of its offspring. Egilmez and Jazwinski first suggested the presence of diffusible cytoplasmic factors in *S. cerevisiae* that were transmitted to progeny before being cleared from one of the latter (Egilmez and Jazwinski, 1989). Asymmetric distribution of aggregated proteins was then reported in *S. cerevisiae* (Aguilaniu et al., 2003; Erjavec et al., 2007) and *E. coli* (Lindner et al., 2008; Winkler et al., 2010), suggested in *C. crescentus* (Ackermann et al., 2003; Shapiro et al., 2002) and documented in mammalian cells (Bufalino et al., 2013; Fuentealba et al., 2008). In *E. coli*, the chaperone IbpA and the disaggregating chaperones DnaK/J/ClpB served as proxies to trace accumulation of protein

aggregates at the old pole (Lindner et al., 2008). Here, we found that a similar process operates in mycobacteria.

We not only used Mtb's chaperone-refoldase ClpB to track IOP but also discovered that ClpB, while non-essential to Mtb in standard growth conditions, plays a critical role in Mtb's recovery from stresses as diverse as late stationary phase, the protein synthesis inhibitors kanamycin and streptomycin, and INH, an inhibitor of mycolic acid synthesis. Moreover, ClpB was essential for Mtb's normal growth and persistence in mice. These disparate conditions may each impose or enhance susceptibility to oxidative stress. In stationary phase, mistranslation promotes improper folding of proteins, which is associated with their oxidation and carbonylation (Ballesteros et al., 2001; Barak et al., 1996; Desnues et al., 2003; Dukan et al., 2000). Similarly, streptomycin—like kanamycin, an aminoglycoside—corrupts ribosomal fidelity and induces mistranslation and protein carbonylation (Dukan et al., 2000). Radical and electrophilic intermediates of INH activation could promote oxidative damage (Njuma et al., 2014). Antibiotics with diverse primary mechanisms of action share the property of disturbing aerobic bacterial metabolism in such a way as to favor generation of hydroxyl radicals (Kohanski et al., 2007). Indeed, oxidative stress contributes to the aerobic killing of Mtb by streptomycin, INH and other antibiotics (Grant et al., 2012; Nandakumar et al., 2014).

Many key questions in bacterial biology involve intra- or inter-cellular heterogeneity and are best answered by comparing individual cells in statistically robust ways. TLM is a powerful tool for addressing such questions as whether differences in growth rates account for phenotypic tolerance to antibiotics (Aldridge et al., 2012; Balaban et al., 2004; Kieser and Rubin, 2014; Wakamoto et al., 2013). The bottleneck of TLM studies remains the difficulty of efficiently and objectively quantifying phenomena at the levels of microcolonies and single cells. Here we have introduced two open-source de-noising plugins to quantitate sequential images of bacteria clusters and adjusted an existing spot detector tool to correct for photobleaching.

We used these computational tools to quantitatively document the distribution of ClpB— a marker of IOP—in response to stresses imposed by two prototypic antibiotics. Combining a fluorescent probe for IOP and a version of Dendra2 that allows photoconversion in mycobacteria, we found that ClpB associates non-covalently and reversibly with aggregates of IOP in mycobacteria, and that the aggregates are reduced in number as they grow in size through coalescence. Coalescence of aggregates limits the exposure of hydrophobic surfaces of mis-folded proteins and minimizes the number of molecules of a chaperone that would be required to coat the aggregates' surface.

Upon cell division, unresolved aggregates were asymmetrically distributed between progeny, whose elongation rate varied inversely with the quantity of aggregated ClpB that they inherited. The inherited burden of aggregates was heterogeneous, conferring on the population a diversity of growth rates. This may prepare different subpopulations to adapt to different environmental conditions, including exposure to antibiotics that are chiefly active against replicating cells (Dhar and McKinney, 2007). Indeed, mycobacteria emerging from a first exposure to kanamycin with lower burdens of IOP were more likely to divide following

a second exposure to kanamycin, while cells with a higher burden of IOP were more likely to lyse or linger without dividing. Fay et al. recently described formation of aggregates of DnaK in stationary phase Msm (Fay and Glickman, 2014). ClpB was observed in association with aggregates when DnaK was depleted or when Msm was transformed with an aggregation sequence fused to a fluorophore. Although the study was not quantitative, DnaK aggregates appeared to be asymmetrically distributed on resumption of replication (Fay and Glickman, 2014).

Parry and colleagues proposed that reduced metabolic activity and other stress conditions trigger a fluid-to-glass-like transition of bacterial cytoplasm, limiting the diffusion of molecules in proportion to their size (Parry et al., 2014). This may be a mechanism underlying our observation that smaller aggregates resolved more often than larger ones. Moreover, in bacteria with reduced metabolism, immobilized large particles can further reduce the mobility of other particles in their neighborhood (Parry et al., 2014). Perhaps when diffusion is most limited at the pole harboring a large aggregate, diffusible components of the cell's elongation and division machineries accumulate at the opposite pole.

Other mechanisms besides the biophysical state of the cytosol may help determine the trafficking and positioning of aggregated IOP. In heat-shocked *E. coli*, the nucleoid excludes protein aggregates from the cell center (Coquel et al., 2013). In yeast, the actin-based cytoskeleton has been implicated in asymmetric distribution of damaged macromolecules (Song et al., 2014). However, mycobacteria do not encode an actin homolog.

ClpB and other molecular players in asymmetric distribution of IOP in mycobacteria may serve as a novel class of targets for the development of drugs that sensitize Mtb to host immune chemistry and to other drugs. To the extent that impaired metabolism both reduces antioxidant defenses in mycobacteria and conduces to their glassification, inhibitors of enzymes such as dihydrolipoamide acyltransferase (Bryk et al., 2008), lipoamide dehydrogenase (Bryk et al., 2013) or isocitrate lyase (Nandakumar et al., 2014) may reduce the ability of mycobacteria to control their IOP.

EXPERIMENTAL PROCEDURES

Procedures for oxidation of BSA, detection of carbonyls, cell fractionation, cross-linking, synthesis of probes for carbonyls, construction of strains, imaging, infection of mice and determination of MICs are described in the Extended Experimental Procedures.

Strains and culture conditions

Table S1 lists strains. Strains were cultured at 37°C in Middlebrook 7H9 with 0.2% glycerol, 0.5% bovine serum albumin fraction V (BSA), 0.02% tyloxapol, 0.2% dextrose, and 0.085% NaCl. Strains bearing antibiotic cassettes were cultured with hygromycin(50 μg/mL), zeocin (25 μg/mL), nourseothricin (25 μg/mL), or streptomycin (25 μg/mL).

Light microscopy and analysis

TLM was performed in a custom-built microfluidic device. Images were processed with the open-source programs ImageJ (http://imagej.nih.gov/ij/) or Icy (http://

icy.bioimageanalysis.org/) using customized plugins, as detailed in Extended Experimental Procedures. Data were compiled using Matlab (The MathWorks).

Supplementary Material

Refer to Web version on PubMed Central for supplementary material.

Acknowledgments

We thank L. Botella, T. Chidawanyika, B. Schwer, K. Rhee, S. Ehrt and K. Burns-Huang (Weill Cornell Medical College), the Bio-Imaging and Proteomics Resource Centers (Rockefeller University),and O. Vandal (Bill and Melinda Gates Foundation) for invaluable help and advice, M. Niki (Osaka City University Graduate School of Medicine) and T. Dick (National University of Singapore School of Medicine) for the HupB knockout, and G. Sukenich of the NMR Analytical Core Facility at MSKCC for NMR and mass spectra. This work was supported by the Bill and Melinda Gates Foundation Grand Challenges Exploration program, the Potts Memorial Foundation and the Milstein Program in Translational Medicine. The Department of Microbiology and Immunology is supported by the William Randolph Hearst Foundation. The Organic Synthesis Core Facility at MSKCC is supported by NCI (grant P30 CA008748-48) and NIH (grant R01 A1064768-09).

References

Ackermann M, Stearns SC, Jenal U. Senescence in a bacterium with asymmetric division. Science. 2003; 300:1920. [PubMed: 12817142]

Aguilaniu H, Gustafsson L, Rigoulet M, Nyström T. Asymmetric inheritance of oxidatively damaged proteins during cytokinesis. Science. 2003; 299:1751–1753. [PubMed: 12610228]

Ahuja SD, Ashkin D, Avendano M, Banerjee R, Bauer M, Bayona JN, Becerra MC, Benedetti A, Burgos M, Centis R, et al. Multidrug resistant pulmonary tuberculosis treatment regimens and patient outcomes: an individual patient data meta-analysis of 9,153 patients. PLoS Med. 2012; 9:e1001300. [PubMed: 22952439]

Aldridge BB, Fernandez-Suarez M, Heller D, Ambravaneswaran V, Irimia D, Toner M, Fortune SM. Asymmetry and aging of mycobacterial cells lead to variable growth and antibiotic susceptibility. Science. 2012; 335:100–104. [PubMed: 22174129]

Balaban NQ, Merrin J, Chait R, Kowalik L, Leibler S. Bacterial persistence as a phenotypic switch. Science. 2004; 305:1622–1625. [PubMed: 15308767]

Ballesteros M, Fredriksson A, Henriksson J, Nyström T. Bacterial senescence: protein oxidation in non-proliferating cells is dictated by the accuracy of the ribosomes. EMBO J. 2001; 20:5280–5289. [PubMed: 11566891]

Barak Z, Gallant J, Lindsley D, Kwieciszewki B, Heidel D. Enhanced ribosome frameshifting in stationary phase cells. J Mol Biol. 1996; 263:140–148. [PubMed: 8913297]

Bryk R, Arango N, Maksymiuk C, Balakrishnan A, Wu YT, Wong CH, Masquelin T, Hipskind P, Lima CD, Nathan C. Lipoamide channel-binding sulfonamides selectively inhibit mycobacterial lipoamide dehydrogenase. Biochemistry. 2013; 52:9375–9384. [PubMed: 24251446]

Bryk R, Gold B, Venugopal A, Singh J, Samy R, Pupek K, Cao H, Popescu C, Gurney M, Hotha S, et al. Selective killing of nonreplicating mycobacteria. Cell Host Microbe. 2008; 3:137–145. [PubMed: 18329613]

Bryk R, Lima CD, Erdjument-Bromage H, Tempst P, Nathan C. Metabolic enzymes of mycobacteria linked to antioxidant defense by a thioredoxin-like protein. Science. 2002; 295:1073–1077. [PubMed: 11799204]

Bufalino MR, DeVeale B, van der Kooy D. The asymmetric segregation of damaged proteins is stem cell-type dependent. J Cell Biol. 2013; 201:523–530. [PubMed: 23649805]

Coelho M, Lade SJ, Alberti S, Gross T, Tolić IM. Fusion of protein aggregates facilitates asymmetric damage segregation. PLoS Biol. 2014; 12:e1001886. [PubMed: 24936793]

Coquel AS, Jacob JP, Primet M, Demarez A, Dimiccoli M, Julou T, Moisan L, Lindner AB, Berry H. Localization of protein aggregation in *Escherichia coli* is governed by diffusion and nucleoid macromolecular crowding effect. PLoS Comput Biol. 2013; 9:e1003038. [PubMed: 23633942]

Darwin KH, Ehrt S, Gutierrez-Ramos JC, Weich N, Nathan CF. The proteasome of *Mycobacterium tuberculosis* is required for resistance to nitric oxide. Science. 2003; 302:1963–1966. [PubMed: 14671303]

de Chaumont F, Dallongeville S, Chenouard N, Hervé N, Pop S, Provoost T, Meas-Yedid V, Pankajakshan P, Lecomte T, Le Montagner Y, et al. Icy: an open bioimage informatics platform for extended reproducible research. Nat Methods. 2012; 9:690–696. [PubMed: 22743774]

Desnues B, Cuny C, Grégori G, Dukan S, Aguilaniu H, Nyström T. Differential oxidative damage and expression of stress defence regulons in culturable and non-culturable *Escherichia coli* cells. EMBO Rep. 2003; 4:400–404. [PubMed: 12671690]

Dhar N, McKinney JD. Microbial phenotypic heterogeneity and antibiotic tolerance. Curr Opin Microbiol. 2007; 10:30–38. [PubMed: 17215163]

Dukan S, Farewell A, Ballesteros M, Taddei F, Radman M, Nyström T. Protein oxidation in response to increased transcriptional or translational errors. Proc Natl Acad Sci U S A. 2000; 97:5746–5749. [PubMed: 10811907]

Dukan S, Nyström T. Bacterial senescence: stasis results in increased and differential oxidation of cytoplasmic proteins leading to developmental induction of the heat shock regulon. Genes Dev. 1998; 12:3431–3441. [PubMed: 9808629]

Dukan S, Nyström T. Oxidative stress defense and deterioration of growth-arrested *Escherichia coli* cells. J Biol Chem. 1999; 274:26027–26032. [PubMed: 10473549]

Egilmez NK, Jazwinski SM. Evidence for the involvement of a cytoplasmic factor in the aging of the yeast *Saccharomyces cerevisiae*. J Bacteriol. 1989; 171:37–42. [PubMed: 2644196]

Erjavec N, Larsson L, Grantham J, Nyström T. Accelerated aging and failure to segregate damaged proteins in Sir2 mutants can be suppressed by overproducing the protein aggregation-remodeling factor Hsp104p. Genes Dev. 2007; 21:2410–2421. [PubMed: 17908928]

Fay A, Glickman MS. An essential nonredundant role for mycobacterial DnaK in native protein folding. PLoS Genet. 2014; 10:e1004516. [PubMed: 25058675]

Fridman O, Goldberg A, Ronin I, Shoresh N, Balaban NQ. Optimization of lag time underlies antibiotic tolerance in evolved bacterial populations. Nature. 2014 advance online publication.

Fuentealba LC, Eivers E, Geissert D, Taelman V, De Robertis EM. Asymmetric mitosis: Unequal segregation of proteins destined for degradation. Proc Natl Acad Sci U S A. 2008; 105:7732–7737. [PubMed: 18511557]

Glover JR, Lindquist S. Hsp104, Hsp70, and Hsp40: a novel chaperone system that rescues previously aggregated proteins. Cell. 1998; 94:73–82. [PubMed: 9674429]

Goloubinoff P, Mogk A, Zvi AP, Tomoyasu T, Bukau B. Sequential mechanism of solubilization and refolding of stable protein aggregates by a bichaperone network. Proc Natl Acad Sci U S A. 1999; 96:13732–13737. [PubMed: 10570141]

Grant SS, Kaufmann BB, Chand NS, Haseley N, Hung DT. Eradication of bacterial persisters with antibiotic-generated hydroxyl radicals. Proc Natl Acad Sci U S A. 2012; 109:12147–12152. [PubMed: 22778419]

Grune T, Jung T, Merker K, Davies KJ. Decreased proteolysis caused by protein aggregates, inclusion bodies, plaques, lipofuscin, ceroid, and 'aggresomes' during oxidative stress, aging, and disease. Int J Biochem Cell Biol. 2004; 36:2519–2530. [PubMed: 15325589]

Gurskaya NG, Verkhusha VV, Shcheglov AS, Staroverov DB, Chepurnykh TV, Fradkov AF, Lukyanov S, Lukyanov KA. Engineering of a monomeric green-to-red photoactivatable fluorescent protein induced by blue light. Nat Biotechnol. 2006; 24:461–465. [PubMed: 16550175]

Hartl FU, Bracher A, Hayer-Hartl M. Molecular chaperones in protein folding and proteostasis. Nature. 2011; 475:324–332. [PubMed: 21776078]

Hill SM, Hao X, Liu B, Nyström T. Life-span extension by a metacaspase in the yeast *Saccharomyces cerevisiae*. Science. 2014; 344:1389–1392. [PubMed: 24855027]

Kieser KJ, Rubin EJ. How sisters grow apart: mycobacterial growth and division. Nat Rev Microbiol. 2014

Kohanski MA, Dwyer DJ, Hayete B, Lawrence CA, Collins JJ. A common mechanism of cellular death induced by bactericidal antibiotics. Cell. 2007; 130:797–810. [PubMed: 17803904]

Lin G, Li D, de Carvalho LP, Deng H, Tao H, Vogt G, Wu K, Schneider J, Chidawanyika T, Warren JD, et al. Inhibitors selective for mycobacterial versus human proteasomes. Nature. 2009; 461:621–626. [PubMed: 19759536]

Lindner AB, Madden R, Demarez A, Stewart EJ, Taddei F. Asymmetric segregation of protein aggregates is associated with cellular aging and rejuvenation. Proc Natl Acad Sci U S A. 2008; 105:3076–3081. [PubMed: 18287048]

Ling J, Cho C, Guo LT, Aerni HR, Rinehart J, Söll D. Protein aggregation caused by aminoglycoside action is prevented by a hydrogen peroxide scavenger. Mol Cell. 2012; 48:713–722. [PubMed: 23122414]

Liu B, Larsson L, Caballero A, Hao X, Oling D, Grantham J, Nyström T. The polarisome is required for segregation and retrograde transport of protein aggregates. Cell. 2010; 140:257–267. [PubMed: 20141839]

Mazloum N, Stegman MA, Croteau DL, Van Houten B, Kwon NS, Ling Y, Dickinson C, Venugopal A, Towheed MA, Nathan C. Identification of a chemical that inhibits the mycobacterial UvrABC complex in nucleotide excision repair. Biochemistry. 2011; 50:1329–1335. [PubMed: 21235228]

Motohashi K, Watanabe Y, Yohda M, Yoshida M. Heat-inactivated proteins are rescued by the DnaK.J-GrpE set and ClpB chaperones. Proc Natl Acad Sci U S A. 1999; 96:7184–7189. [PubMed: 10377389]

Nandakumar M, Nathan C, Rhee K. Isocitrate lyase mediates broad antibiotic tolerance *Mycobacterium tuberculosis*. Nature Communications. 2014

Njuma OJ, Ndontsa EN, Goodwin DC. Catalase in peroxidase clothing: Interdependent cooperation of two cofactors in the catalytic versatility of KatG. Arch Biochem Biophys. 2014; 544C:27–39.

Olivo-Marin JC. Extraction of spots in biological images using multiscale products. Pattern Recognition. 2002; 35:1989–1996.

Parry BR, Surovtsev IV, Cabeen MT, O'Hern CS, Dufresne ER, Jacobs-Wagner C. The Bacterial Cytoplasm Has Glass-like Properties and Is Fluidized by Metabolic Activity. Cell. 2014; 156:183–194. [PubMed: 24361104]

Raju RM, Unnikrishnan M, Rubin DH, Krishnamoorthy V, Kandror O, Akopian TN, Goldberg AL, Rubin EJ. *Mycobacterium tuberculosis* ClpP1 and ClpP2 function together in protein degradation and are required for viability in vitro and during infection. PLoS Pathog. 2012; 8:e1002511. [PubMed: 22359499]

Rosenzweig R, Moradi S, Zarrine-Afsar A, Glover JR, Kay LE. Unraveling the mechanism of protein disaggregation through a ClpB-DnaK interaction. Science. 2013; 339:1080–1083. [PubMed: 23393091]

Santi I, Dhar N, Bousbaine D, Wakamoto Y, McKinney JD. Single-cell dynamics of the chromosome replication and cell division cycles in mycobacteria. Nat Commun. 2013; 4:2470. [PubMed: 24036848]

Shapiro L, McAdams HH, Losick R. Generating and exploiting polarity in bacteria. Science. 2002; 298:1942–1946. [PubMed: 12471245]

Song J, Yang Q, Yang J, Larsson L, Hao X, Zhu X, Malmgren-Hill S, Cvijovic M, Fernandez-Rodriguez J, Grantham J, et al. Essential Genetic Interactors of SIR2 Required for Spatial Sequestration and Asymmetrical Inheritance of Protein Aggregates. PLoS Genet. 2014; 10:e1004539. [PubMed: 25079602]

Takatsuka M, Osada-Oka M, Satoh EF, Kitadokoro K, Nishiuchi Y, Niki M, Inoue M, Iwai K, Arakawa T, Shimoji Y, et al. A histone-like protein of mycobacteria possesses ferritin superfamily protein-like activity and protects against DNA damage by Fenton reaction. PLoS One. 2011; 6:e20985. [PubMed: 21698192]

Tamarit J, Cabiscol E, Ros J. Identification of the major oxidatively damaged proteins in *Escherichia coli* cells exposed to oxidative stress. J Biol Chem. 1998; 273:3027–3032. [PubMed: 9446617]

Tiemersma EW, van der Werf MJ, Borgdorff MW, Williams BG, Nagelkerke NJ. Natural history of tuberculosis: duration and fatality of untreated pulmonary tuberculosis in HIV negative patients: a systematic review. PLoS One. 2011; 6:e17601. [PubMed: 21483732]

Wakamoto Y, Dhar N, Chait R, Schneider K, Signorino-Gelo F, Leibler S, McKinney JD. Dynamic persistence of antibiotic-stressed mycobacteria. Science. 2013; 339:91–95. [PubMed: 23288538]

Weibezahn J, Tessarz P, Schlieker C, Zahn R, Maglica Z, Lee S, Zentgraf H, Weber-Ban EU, Dougan DA, Tsai FT, et al. Thermotolerance requires refolding of aggregated proteins by substrate translocation through the central pore of ClpB. Cell. 2004; 119:653–665. [PubMed: 15550247]

Winkler J, Seybert A, König L, Pruggnaller S, Haselmann U, Sourjik V, Weiss M, Frangakis AS, Mogk A, Bukau B. Quantitative and spatiotemporal features of protein aggregation in *Escherichia coli* and consequences on protein quality control and cellular ageing. EMBO J. 2010; 29:910–923. [PubMed: 20094032]

Winter J, Linke K, Jatzek A, Jakob U. Severe oxidative stress causes inactivation of DnaK and activation of the redox-regulated chaperone Hsp33. Mol Cell. 2005; 17:381–392. [PubMed: 15694339]

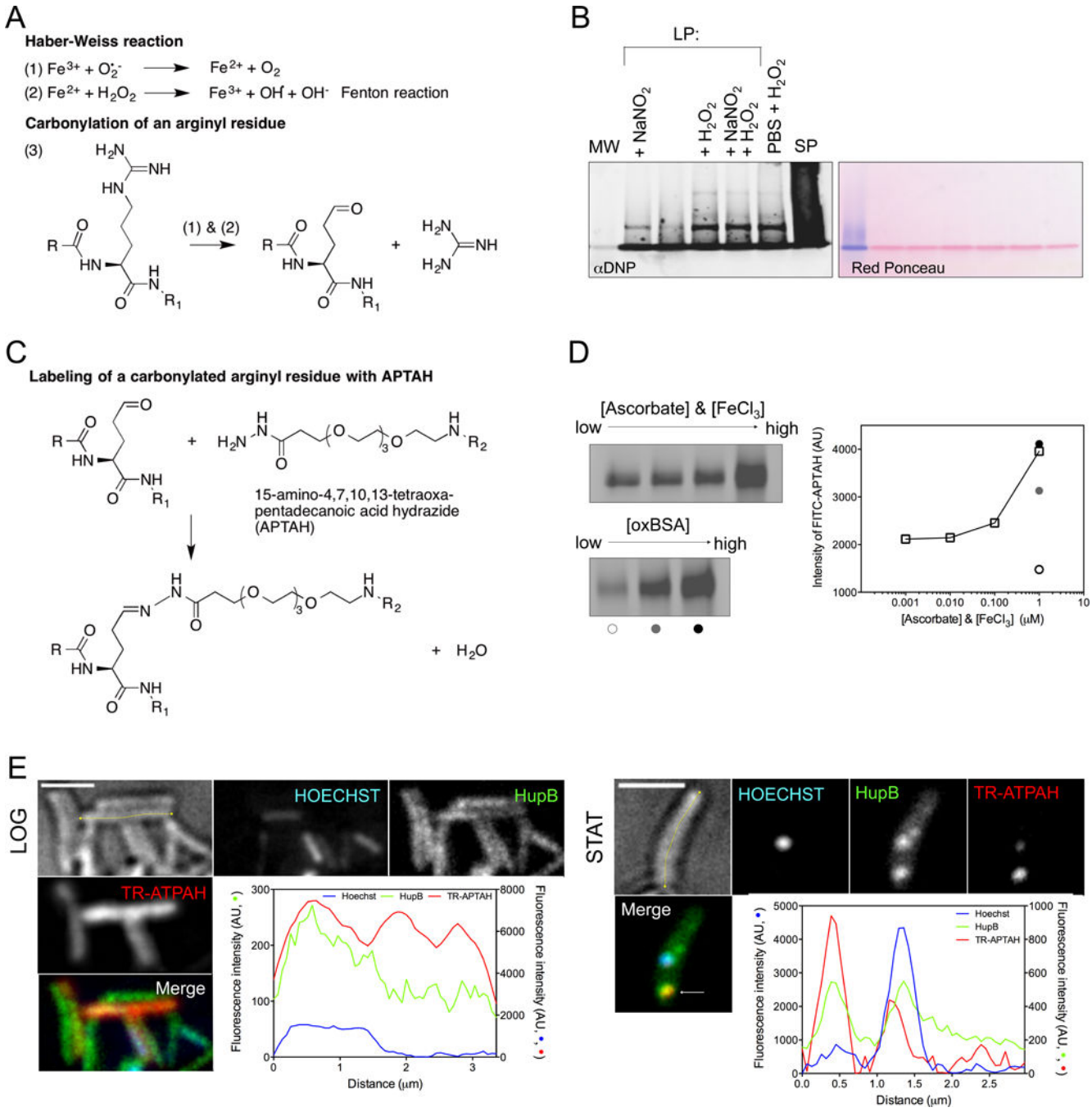

Figure 1. Proteomic analysis of Mtb's IOP, see also Figure S1

(A) Haber-Weiss chemistry ((1) and (2)) drives OH• generation and addition of carbonyls on amino acid side chains, e.g. an arginyl residue (3).

(B) DNPH-reacted protein samples from Mtb in logarithmic phase (LP) from cultures that were: untreated or supplemented with $NaNO_2$ (3 mM, pH 5.5), H_2O_2 (5 mM), or a combination of nitrite (0.5 mM) and H_2O_2 (2.5 mM) at pH 5.5; or subjected to starvation for 1 to 2 weeks in phosphate buffered saline (PBS) and H_2O_2 (5 mM); or from Mtb in stationary phase (SP) (left panel). Hydrazone derivatives were blotted with anti-DNP

antibody. Ponceau red staining served as a loading control (right panel). MW, molecular weight controls that migrated in a single band on 5% SDS stacking gel.
(C) Reaction of fluorophore-derivatized 15-amino-4,7,10,13-tetraoxapentadecanoic acid hydrazide (ATPAH) with carbonyls. R and R_1 indicate the N- and C- termini of a protein. R_2 represents FITC or Texas red.
(D) Reaction of probe in (C) with oxidized BSA. The amount of staining (first 4 lanes of (D, left)) increased with the concentration of the oxidant pair $FeCl_3$ and ascorbic acid, incubated for 12 h in the equimolar concentrations indicated in (D, right) with BSA. Staining also increased with the quantity of oxidized BSA (125, 250 and 500 ng) as indicated by the open, gray and black circles below the 3 lanes of (D, bottom left) and quantified in (D, right).
(E) Intracellular distribution of HupB, a carbonylated protein, as a fusion with Dendra2 in relation to its carbonylation status (TR-APTAH stain) and the nucleoid (Hoechst) in logarithmic (LOG) and stationary phase (STAT). Intensity of fluorescence (AU) in the 3 channels is quantified along the longitudinal axis (yellow) of representative cells. Inspection of z-planes showed that bright TR-APTAH staining of some LOG cells came from the cell surface. Scale bar, 2 microns.

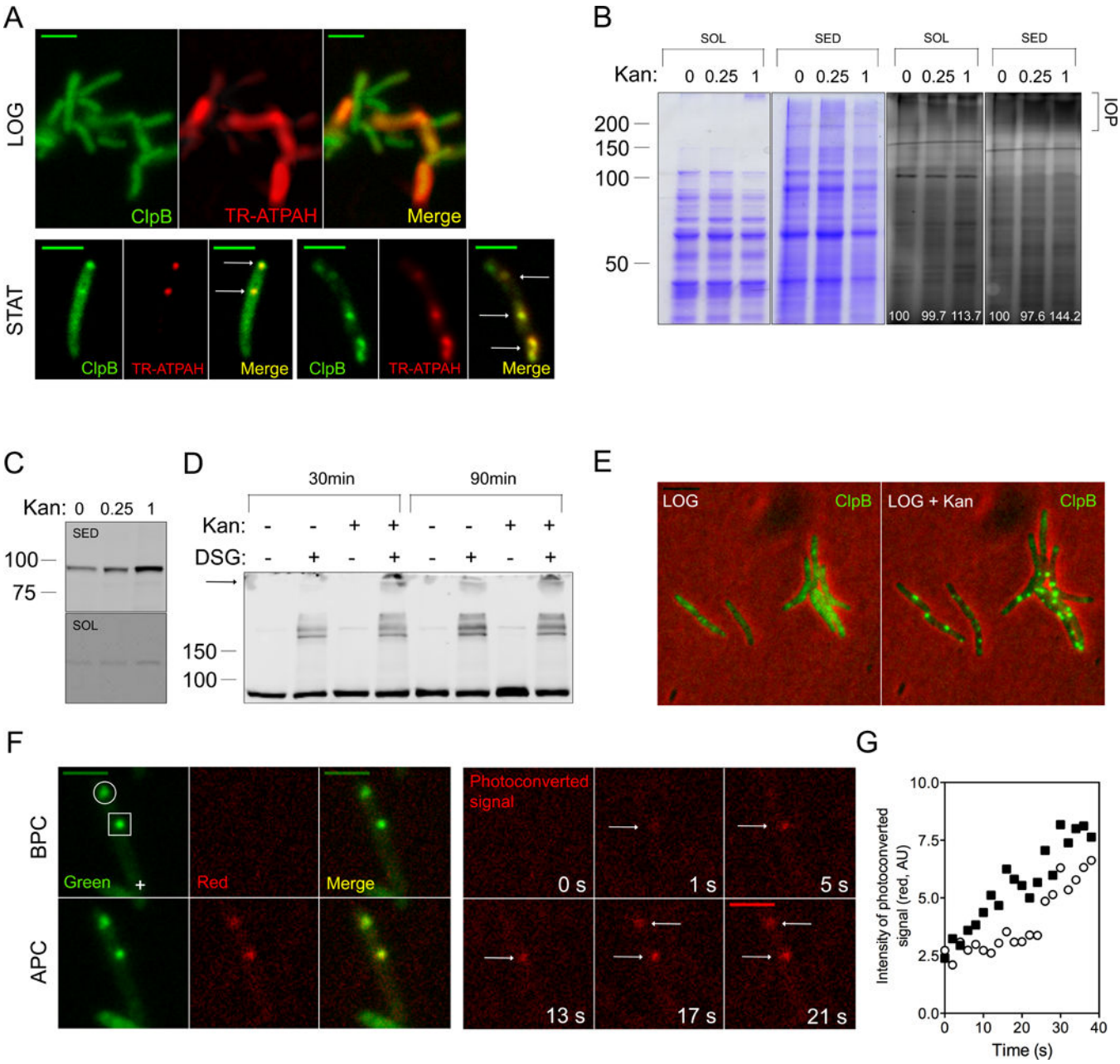

Figure 2. ClpB largely co-localizes with IOP, see also Figures S2 and S3

(A) Distribution of ClpB-GFP (green) and carbonyls reactive with TR-ATPAH (red) in Mtb in logarithmic phase (LOG) and stationary phase (STAT). Scale bar, 2 microns for the last row, 4 microns in other micrographs.

(B) Protein carbonylation in Msm subjected to indicated concentrations of kanamycin (μg/mL) prior to fractionation into soluble (SOL) and sedimentable (SED) fractions and reacted with FITC-APTAH prior to SDS-PAGE. Gels were stained with Coomassie (two gels on left) or laser-illuminated (480 nm) (two gels on right). Higher Mr species marked "IOP" may correspond to cross-linked aggregates. Number in white indicate the intensity of the FITC-APTAH signal (AU).

(C) Redistribution of ClpB-GFP into the sedimentable fraction following exposure of Msm to kanamycin. ΔClpBsm::ClpBsm-GFP cells were exposed for 3 h to kanamycin at indicated concentrations prior to fractionation and immunoblotting.

(D) Association of ClpB with higher-Mr protein complexes following kanamycin treatment of Msm. ΔClpBsm::ClpBsm cells were treated with 1 μg/mL of kanamycin for 30 or 90 min and then exposed or not to the cross-linking agent DSG. ClpB-GFP was detected by immunoblot in unfractionated extracts. The arrow indicates the slowest bands emerging preferentially upon kanamycin treatment.

(E) Redistribution of diffuse ClpB-GFP to aggregates in response to sublethal kanamycin. Scale bar, 4 μm.

(F) Entry of ClpB into focal structures in kanamycin-treated Msm. A Msm::ClpB-Dendra2 cell that was treated with 1 μg/mL kanamycin for 2 h contained two focal accumulations of ClpB (open circle and open square, top panel). A region distant from both foci (cross) was illuminated with a 405-nm laser. Dendra2 fluoresced in the green channel (“Green”) before photoconversion (BPC), and in the red channel (“Red”) after photoconversion (APC). Micrographs in the red channel were taken at time 0 and 5, 9, 13, 17 and 21 sec after photoconversion (F, right).

(G) Quantitative representation of the entry of ClpB from the irradiated site in the cell in (F) into the foci indicated by the square and the circle in (F). New molecules of ClpB joined the nearer focus first.

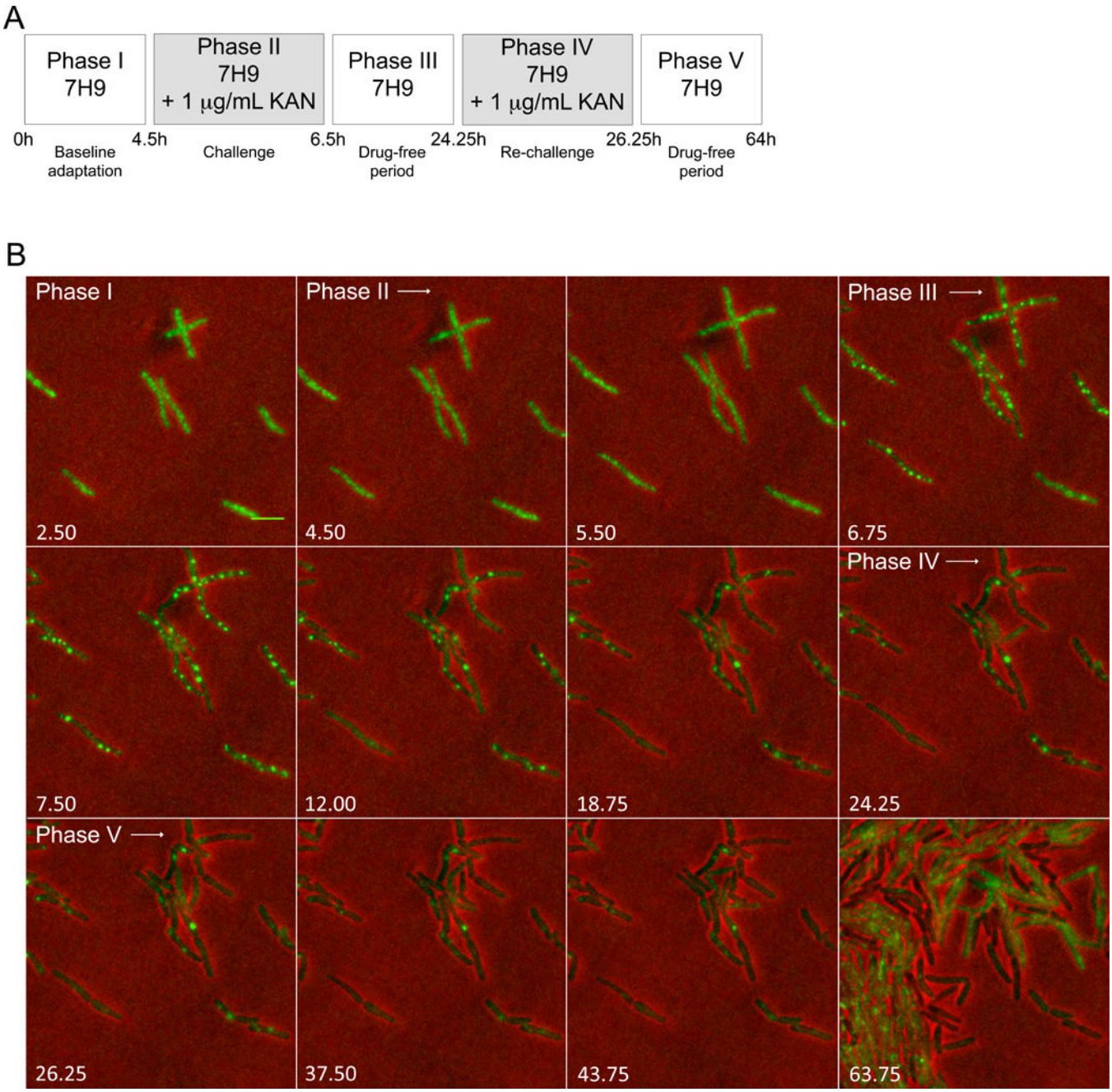

Figure 3. ClpB-Dendra2 foci form in response to sublethal kanamycin

(A) Perfusion paradigm. 7H9, Middlebrook 7H9 medium. KAN, kanamycin (1 μg/mL).

(B) Representative image series for phases defined in (A). Numbers indicate time in hours. Scale bar, 2 μm. Diffuse ClpB redistributed into aggregates upon exposure of Msm to kanamycin. Aggregates later decreased in number. 256 micrographs were recorded over 64 h at constant Illumination.

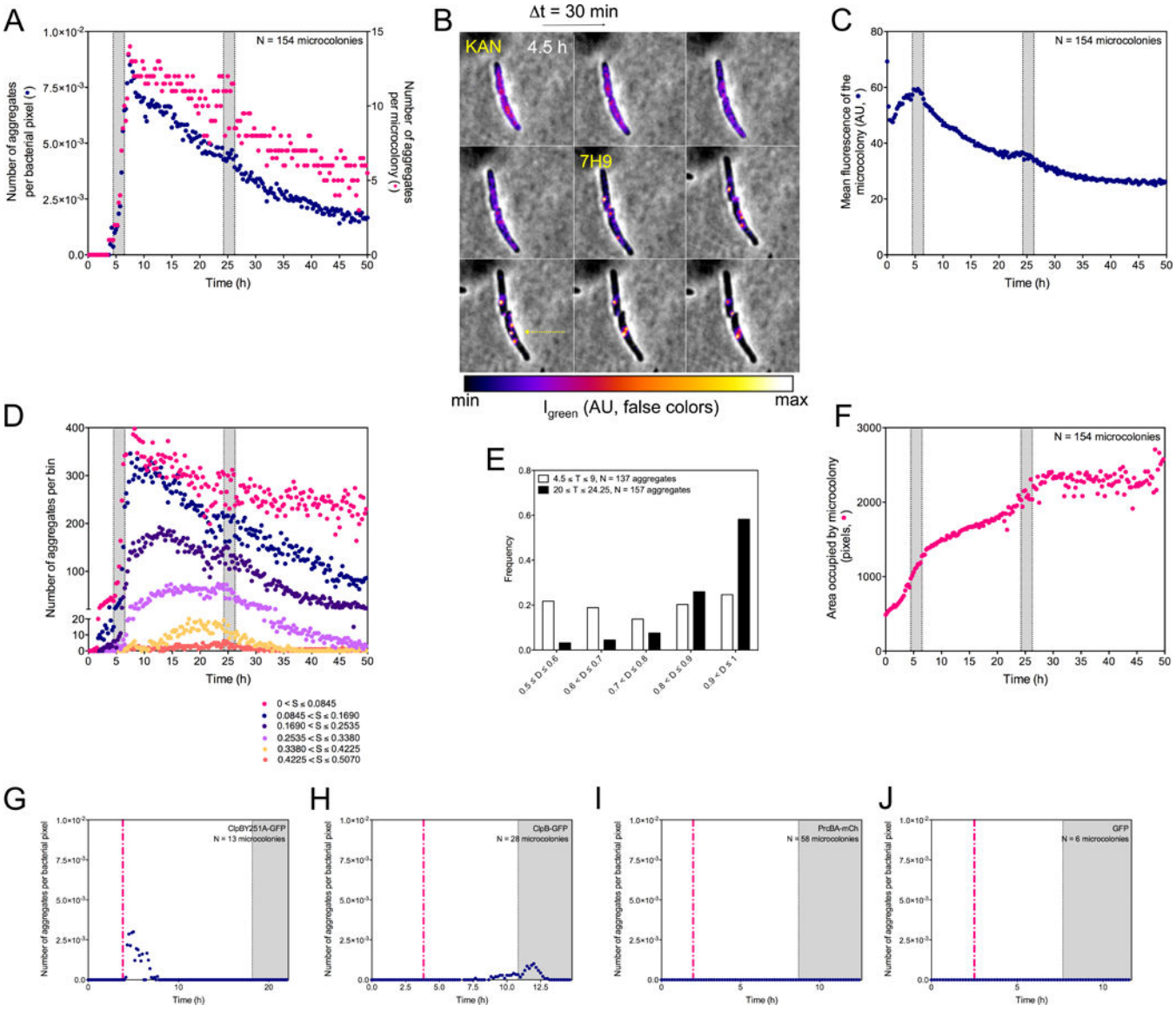

Figure 4. Quantitative characterization of ClpB's association with aggregates in response to kanamycin at the microcolony level, see also Figure S4

(A, C, D, F, G, H, I and J) Shaded areas indicate incubation of Msm with 1 μg/mL kanamycin (panels A, C, D and F) or 0.1 μg/mL (panels G to J). The same 154 microcolonies were analyzed in (A), (C), (D), (E) and (F). Results in (A), (C), (D), (E) and (F) are compiled from 3 experiments. They are representative of results in >15 additional experiments conducted with variations in the timing of perfusion phases, doses of kanamycin or choice of fluorescent tag. (A) Numbers of aggregates per bacterial pixel over time (blue circles) and numbers of aggregates per microcolony (red circles).

(B) Representative image series (Δt = 30 min) of 2 Δ*clpBSm*::*clpB-dendra2* cells over 4 h following exposure to 1 μg/mL of kanamycin. Quantitated, false-color fluorescence images superimposed on phase contrast images illustrate an initially relatively diffuse distribution of ClpB-GFP, followed by its accumulation into aggregates in conjunction with its

disappearance from the intervening volume of the cell. The upper cell develops 2 aggregates; the lower cell develops 3 that fuse into 1.

(C) Mean fluorescence intensity of microcolonies. The mean intensity of fluorescence of bacterial pixels (navy blue) was corrected for photobleaching as in Figure S5A.

(D) Numbers of aggregates of different sizes (S) over time.

(E) Tendency of ClpB-associated aggregates to collect at a pole. The histogram represents the frequency distribution (y-axis) of aggregates' localization in Δ*clpBSm*::*clpB-dendra2* as a function of time in relation to kanamycin exposure on the long axis of each cell, where distances (D) of 0.50 and 1.00 on the x-axis represent mid-cell and a cell pole, respectively. T = time period analyzed in hours.

(F) Growth of microcolonies. The number of bacterial pixels (red circles) was summed over time.

(G to J) Numbers of aggregates per bacterial pixel over time (purple circles). Expression of fluorescent controls was induced by pulse perfusion with Atc (dashed red line; 200 ng/mL).

(G) Failure of ClpBY251A-GFP to enter aggregates in response to 0.1 μg/mL of kanamycin. Transient appearance of fluorescent patches after Atc was attributable to the fluorescence of Atc.

(H) Tendency of ClpB-GFP expressed in Msm with strictly similar genetic background as in (G) to enter aggregates in response to 0.1 μg/mL of kanamycin.

(I) Failure of PrcA-mCherry to enter aggregates in response to 0.1 μg/mL of kanamycin. Msm expressed PrcA-mCherry and PrcB (heptamers in stacks of 4) in response to pulse perfusion with Atc.

(J) Failure of GFP not fused with ClpB to enter aggregates in response to 0.1 μg/mL of kanamycin.

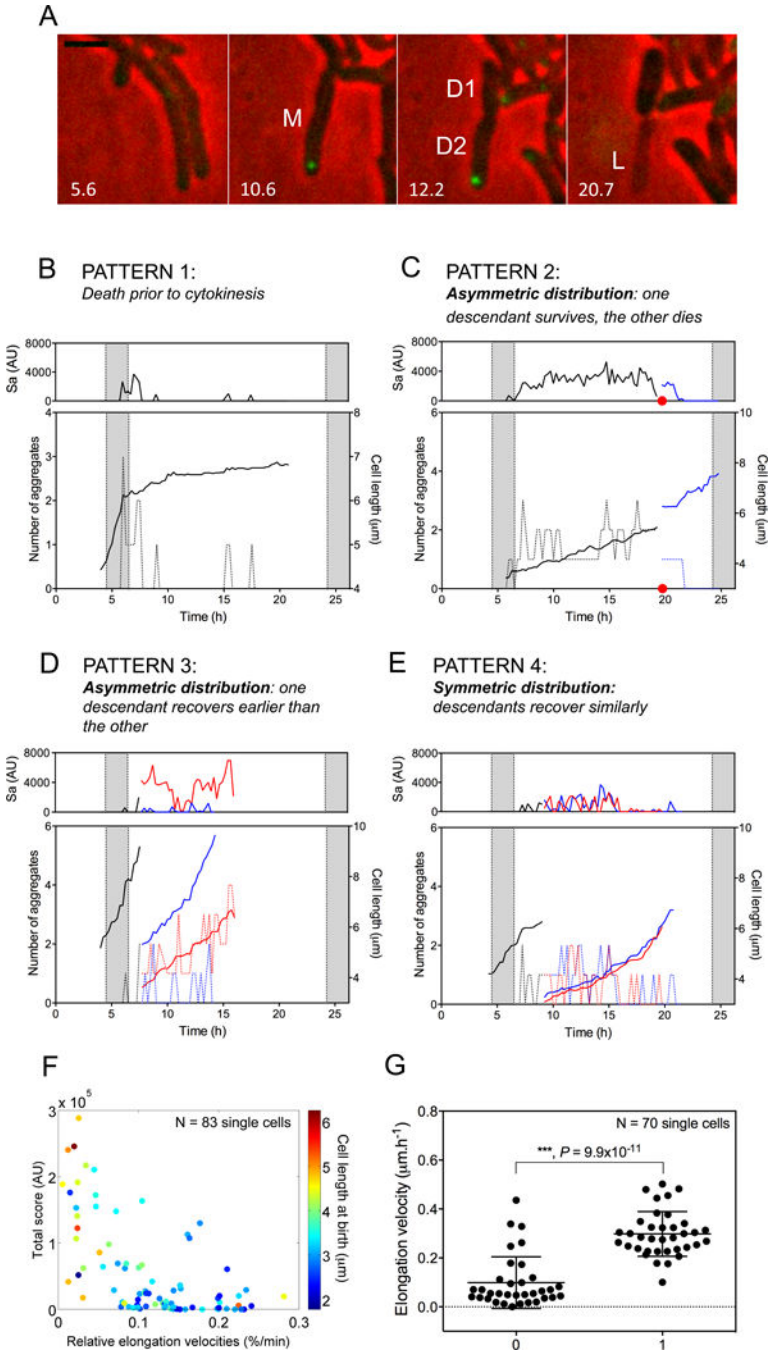

Figure 5. Distribution of ClpB into aggregates within mycobacteria leads to asymmetric distribution of aggregates between their progeny

(A) Photomicrographic evidence. Aggregates accumulate at the cell pole in the parental Msm cell (M) in response to exposure to kanamycin. After removal of kanamycin, M divides. Descendant D1 inherits no aggregates and survives; descendant D2 inherits the ClpB-GFP aggregate and lyses (L). Numbers indicate time in hours. Scale bar, 2 μm. (B–E). Fluctuation in number of aggregates in individual Msm cells and relation of aggregate burden to growth rate. Top panels, aggregate burden (sum of Sa), representing

total fluorescent intensity (AU) of aggregates. Lower panels, number of aggregates (dashed lines) and cell length (μm). Black line, parental cell; red and blue lines, progeny.
(B) Example of a cell that failed to give IOP to progeny and died, losing fluorescence.
(C, D) Examples of cells whose progeny received markedly different burdens of IOP, with the more heavily burdened descendant dying ((C); red dot denotes lysis at the time of division of the parental cell) or growing much more slowly than its less burdened sibling (D).
(E) Example of cells that bestowed nearly equal burdens of IOP on their progeny, whose growth rates were then almost the same.
(F) Relative mean elongation velocity of progeny of stressed parents correlated negatively with their cumulative Sa and with their length at birth (see text).
(G) Ability of cells to divide after a second exposure to kanamycin correlated with their rate of elongation (Y-axis) before the second exposure. X-axis: “0” denotes cells that failed to divide following the second kanamycin exposure; “1” indicates cells that divided at least once during the subsequent drug-free perfusion.

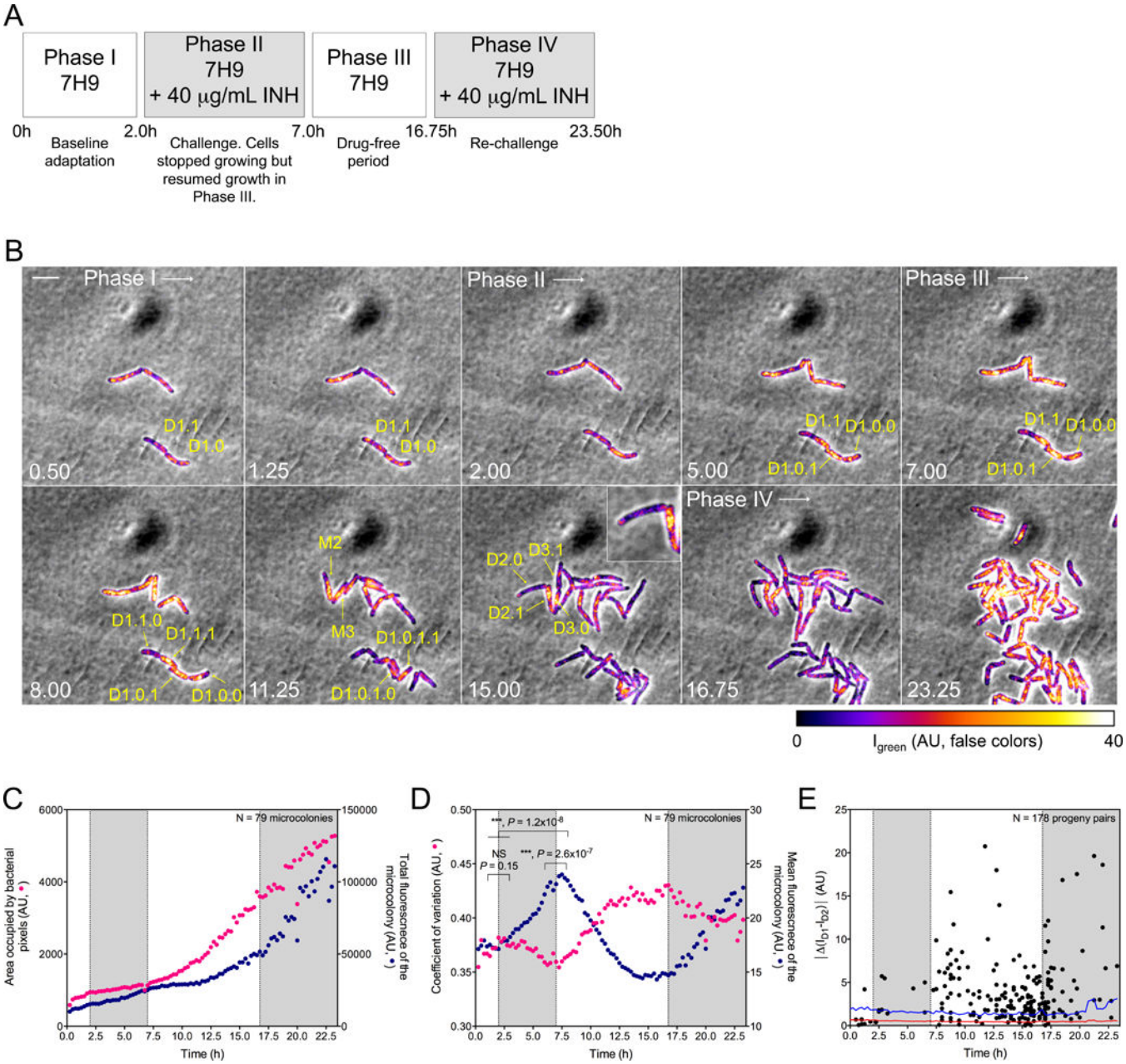

Figure 6. Heterogeneous distribution of ClpB-GFP within mycobacteria and between their progeny in response to a sublethal concentration of INH

(A) Perfusion paradigm. 7H9, Middlebrook 7H9 medium. INH, isoniazid (40 μg/mL). Shaded phases II and IV correspond to shading in panels (C–E).

(B) Representative image series for each phase in (A). Numbers indicate time in hours. Scale bar, 4 μm. False-colored fluorescence intensity, corrected for photobleaching, Decimals denote lineages of parental cells (M) and their descendants (D). Thus, M1's descendant D1.1 gave rise to D1.1.0, which inherited few patches of ClpB, and D1.1.1, which inherited most of the patches of ClpB. Likewise, D2.0 inherited almost no detectable ClpB from M2, while D2.1 (see inset) inherited almost all of it. Results were similar for the descendants of M3.

(C) Relation of microcolony growth to expression of ClpB-GFP. Median growth of 79 microcolonies (yellow circles; total bacterial pixels) is shown on a linear scale in relation to incubation with INH. Summed intensity of ClpB-GFP fluorescence is denoted on a linear scale by blue circles (AU). Total expression of ClpB-GFP increased much more slowly than microcolony biomass, but increased fastest when colony growth slowed.
(D) Quantitative characterization of formation of ClpB-GFP into patches following exposure of Msm microcolonies to INH. As mean fluorescence (fluorescence intensity divided by bacterial pixels; blue circles) of the microcolonies decreased, the median coefficient of variation (σ/μ) of the mean fluorescence increased (red circles). Significance was evaluated by Kolmogorov-Smirnov test for continuous distribution as the null hypothesis.
(E) Quantitative characterization of asymmetric distribution of patched ClpB to progeny following exposure of Msm to sublethal INH. Each dot corresponds to the absolute value of the difference in ClpB fluorescence mean intensities at birth ($|\Delta M_{D1}-|_{D2})|$) between members of a progeny pair, I_{D1} and I_{D2}. This is compared to the mean (red line) of the difference in background fluorescence, calculated as the difference in fluorescence mean intensities of two adjacent areas that were external to cells, identical to each other in size, and similar in size to a bacterium. This background value was calculated every 15 min over 23.5 h for 17 movies from 3 independent experiments. Blue line indicates a confidence level > 99.9% ($p < 0.004$).

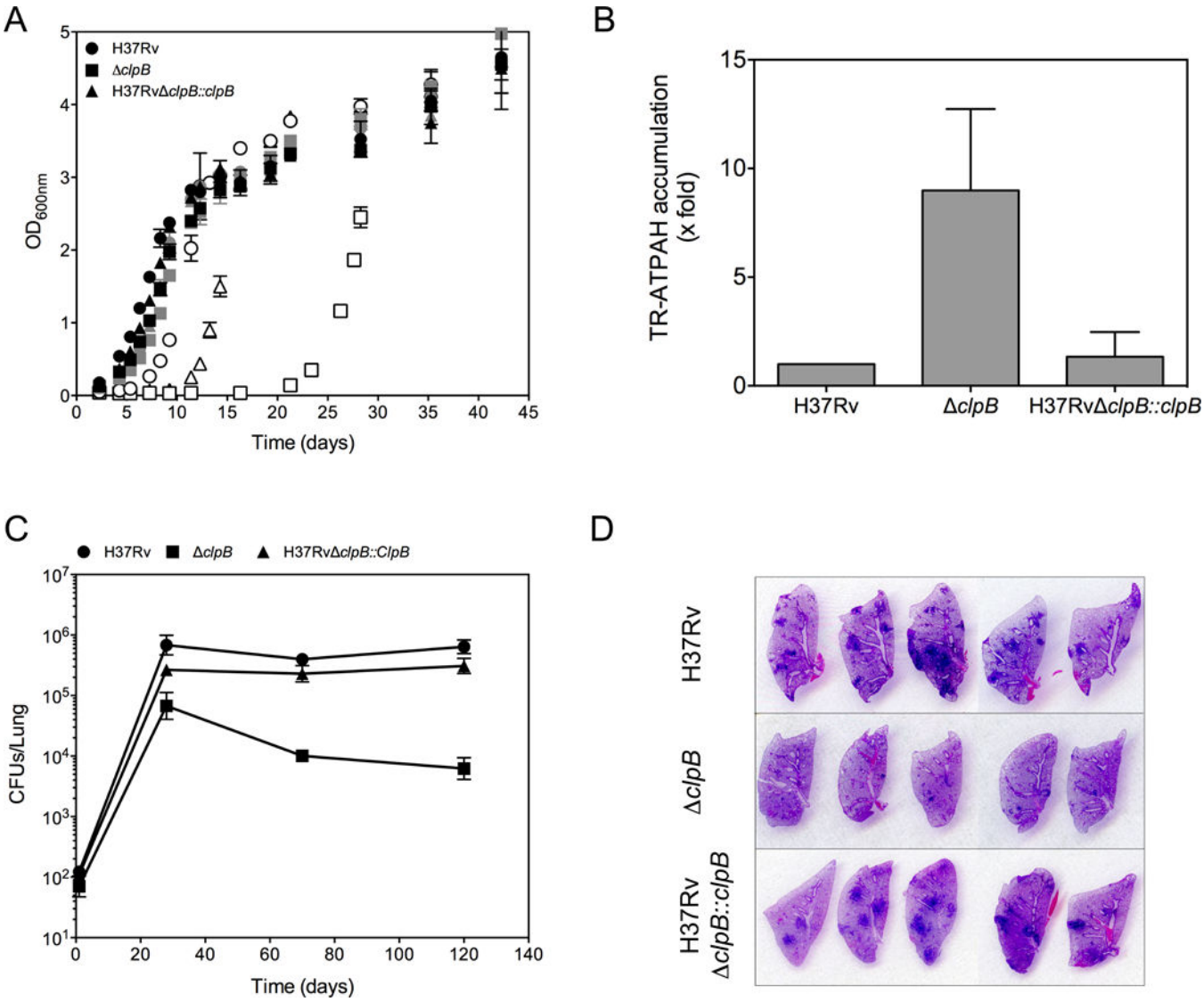

Figure 7. Contribution of ClpB to Mtb's fitness, see also Figure S5

(A) Defective recovery of ClpB-deficient Mtb from stationary phase. Growth of H37Rv (circles), H37RvΔ*clpB* (squares) and the complemented strain H37RvΔ*clpB::clpB* (triangles) in 7H9 medium using inocula from logarithmic phase (black), early stationary phase (gray) or late stationary phase (open symbols). Mean ± SD of 2 experiments, each in duplicate.

(B) Excessive accumulation of carbonyls in ClpB-deficient Mtb in stationary phase. ATPAH reactivity (arbitrary fluorescence units) was compared in late stationary phase in H37RvΔ*clpB* and H37RvΔ*clpB::clpB* cells relative to that in wild type H37Rv, which was set to 1. Mean ± SD of 4 experiments, each in duplicate.

(C) Attenuation of ClpB-deficient Mtb in mice. Colony-forming units (CFU) of H37Rv (circles), H37RvΔ*clpB* (squares) and H37RvΔ*clpB::clpB* (triangles) in lungs of C75BL/6 mice at the indicated times after aerosol infection. Means ± SD for 5 mice per time point from one experiment representative of 2.

(D) Diminished histopathology caused by ClpB-deficient Mtb. Sections of lungs collected at day 120 from mice infected with the indicated strains were stained with hematoxylin and eosin. Photographs show the sections at their actual size.